

Local Clustering for Lung Cancer Image Classification via Sparse Solution Technique

Jackson Hamel* Ming-Jun Lai[†] Zhaiming Shen[‡] Ye Tian[§]

July 28, 2024

Abstract

In this work, we propose to use a local clustering approach based on the sparse solution technique to study the medical image, especially the lung cancer image classification task. We view images as the vertices in a weighted graph and the similarity between a pair of images as the edges in the graph. The vertices within the same cluster can be assumed to share similar features and properties, thus making the applications of graph clustering techniques very useful for image classification. Recently, the approach based on the sparse solutions of linear systems for graph clustering has been found to identify clusters more efficiently than traditional clustering methods such as spectral clustering. We propose to use the two newly developed local clustering methods based on sparse solution of linear system for image classification. In addition, we employ a box spline-based tight-wavelet-framelet method to clean these images and help build a better adjacency matrix before clustering. The performance of our methods is shown to be very effective in classifying images. Our approach is significantly more efficient and either favorable or equally effective compared with other state-of-the-art approaches. Finally, we shall make a remark by pointing out two image deformation methods to build up more artificial image data to increase the number of labeled images.

Key words: Graph Laplacian, Image Simplification, Local Clustering, Lung Cancer Image Classification, Sparse Solution Technique

1 Introduction

Lung cancer is one of the most common, and one of the deadliest cancers; only about 17% of people in the U.S. diagnosed with lung cancer survive five years after the diagnosis. Currently, diagnostic methods to detect this cancer include biopsies and imaging, like CT scans. Given the severity of the cancer, early detection significantly improves the chances for survival, but it is also more difficult to detect early stages of lung cancer as there are typically fewer symptoms. To add to the difficulty and complexity, when imaging techniques display cancerous-looking growths, they could either be benign (not harmful) or malignant (harmful). Thus, our task is a ternary classification problem to detect the presence of lung cancer in a patient's CT scans and determine whether a growth is benign or malignant.

*jrhamel314@uga.edu. Department of Mathematics, University of Georgia, Athens, GA 30602.

[†]mjlai@uga.edu. Department of Mathematics, University of Georgia, Athens, GA 30602. This author is supported by the Simons Foundation Collaboration Grant #864439.

[‡]zhaiming.shen@uga.edu. Department of Mathematics, University of Georgia, Athens, GA 30602.

[§]yt95681@uga.edu. Department of Mathematics, University of Georgia, Athens, GA 30602.

We are interested in lung cancer image classification and providing a complementary method to help computer-aided clinic diagnosis (CACD). More precisely, we would like to help improve the computational feasibility, interpretability, and robustness of the existing methods in image-based CACD. The medical image analysis for lung cancer classification involves two types of approaches: traditional machine learning algorithms, which classify cancer based on manually extracted features from the images, and deep learning techniques, which automatically learn and extract features directly from the raw images. So far, the most popular methods to classify images are based on neural network structures such as ResNet50, EfficientNetB0, InceptionV3, MobileNetV2, DenseNet121, ResNet101, VGG18. See, e.g., [35], [12], [3], [25] for more details. In addition, topological machine learning algorithms such as [2] and [31] were recently developed to provide additional competitive and complementary methods. There are many other algorithms available in the literature and existed online.

The primary objective of this study is to detect cancerous cells in lung nodule CT scan images. It aims to classify lung cancer into three distinct categories: benign, malignant, and normal, based on CT scan slices of lung nodules. To accomplish this task, we propose to use a simple yet effective local clustering approach based on the sparse solution of linear system for image classification. Our idea is based on the methods recently developed in [18], [20], [28]. See [27] for a comprehensive study of these methods.

The main idea of these methods is that we view a set of image data as a graph G whose vertices are associated with images. Images in the same cluster are in the same class, e.g. benign, or malignant or normal. Given a testing (query) image, we look for a cluster, usually of a small size, which contains the query image as the seed. For example, suppose the output cluster (excluding the query image) is of size 6, then if all 6 images belong to one of the three classes, say malignant, the query image is concluded to be a malignant image. Of course, we can also use a weaker criterion: the testing image is malignant if 3 out of the 6 images are malignant, 2 out of the 6 images are benign, 1 out of the 6 images are normal.

To perform the clustering task, the first and foremost step is to build up an effective adjacency matrix for the group of training images. There are a lot of distance functions we can use. As one needs to find the best one in the sense that for the graph only based on labeled sample images, the adjacency matrix should have a block diagonal structure after the permutation according to the class membership. The way to generate a good adjacency matrix is introduced in Section 3 with more details. We will also present a box spline based on tight-wavelet frames (TWF) to simplify all the images by removing some redundant information away so that the adjacency matrix built by a traditional modified exponential distance (cf. [34]) is much cleaner. The idea about image simplification is explained in Section 2.

After building up the adjacency matrix, we simply form its graph Laplace matrix and use our local clustering techniques based on sparse solutions of linear system (cf. [22]). Our idea can be explained as follows. Letting \mathbf{c}_1 be the indicator vector of cluster C_1 whose entries are 1 associated with the vertices in the cluster C_1 , and 0 otherwise. It is easy to see that \mathbf{c}_1 is a sparse vector. For example, the cluster C_1 may have $\|\mathbf{c}_1\|_0 = 5$ while the total number of images is possibly $N \gg 1000$. Thus, the number of nonzero entries in C_1 , i.e. $\|\mathbf{c}_1\|_0$ is much smaller than the size N of the graph. Since we have

$$\mathcal{L}\mathbf{c}_1 = 0, \tag{1}$$

where \mathcal{L} is the graph Laplacian of the graph G (cf. [6]), we cast the problem of finding \mathbf{c}_1 as a minimization problem

$$\min \|\mathbf{x}\|_0, \mathcal{L}\mathbf{x} = 0, \mathbf{x} \neq \mathbf{0}, \tag{2}$$

where $\|\mathbf{x}\|_0$ stands for the number of nonzero entries in \mathbf{x} . This problem was studied two decades ago (cf. [7] and [10]) as a compressive sensing problem. See also [22] for a detailed explanation. In

this paper, we will present two computational algorithms specific to the local clustering problem for identifying lung cancer images. See Section 4 for a detailed explanation.

We shall first demonstrate the effectiveness of these two computational algorithms in categorizing images of various human faces based on two well-known human face datasets: AT&T and YaleB human face data. Then we will show the proposed two algorithms work well for the medical image datasets we studied in this paper. One of the major advantages of our approach is its computational efficiency, as our approach only involved in finding a sparse solution of the linear system associated with the graph Laplacian matrix. It does not need to compute the eigenvectors of the graph Laplacian matrix, which will be more costly when the size of the image data is large. Our numerical experiment can be done in minutes while a convolutional neural network requires hours or more. We summarize our experimental results in Section 5.

The goal of our research is to determine a testing image as one of the three classes: Benign, Malignant, or Normal. Let us first summarize our computational procedure as follows:

- Preprocess the images by rescaling the images to the same size and applying a Gaussian blur algorithm to reduce the high-frequency components of these images.
- Simplify these images by using, e.g. PCA, TWF, Watershed, etc..
- Build up an adjacency matrix A by using, e.g. K-NN, L^2 distance, modified exponential distance.
- For each testing image, we use either one of the two proposed local clustering methods, Local Cluster Extraction (LCE) or Least Squares Clustering (LSC), to find a small cluster of images which are similar to the given testing image.
- Make conclusion about the label of the testing image based on the majority vote of the labels of the images in the found small cluster.

We shall explain these steps of computation in the following sections. The main contributions of this work are the following:

- We propose to use an approach based on the idea of sparse solution technique for local clustering in order to identify a given test image is benign, malignant, or normal.
- We treat each image as a vertex in the graph, and use modified exponential distance to build the adjacency matrix between all pairs of images. Then we apply LCE or LSC for medical image classification (identification).
- The image is preprocessed by applying a box spline based tight-wavelet frames method, with edgeS being detected and enhanced.
- The experiments demonstrate that our image classification is fast and accurate, and hence can be served as a complementary method to help CACD.

However, we notice that the size of the data set we are using is small, about 1097 images. In order to achieve a better result, we can increase the size of the labeled data. We will propose two approaches: one is based on the solution of the optimal transport problem, i.e. a numerical approximation of the minimizer based on the solution of Monge-Ampère equation studied in [17] to help generate more labeled images. The other approach is based on harmonic generalized barycentric coordinates (GBC) for image deformation (cf. [9]). We will show a few examples to illustrate the GBC approach for generating more labeled images in the end of the paper while leaving the entire computation of generating new images to the future work. Nevertheless, we will remark in Section 6 to convince the readers that this approach will generate enough labeled data.

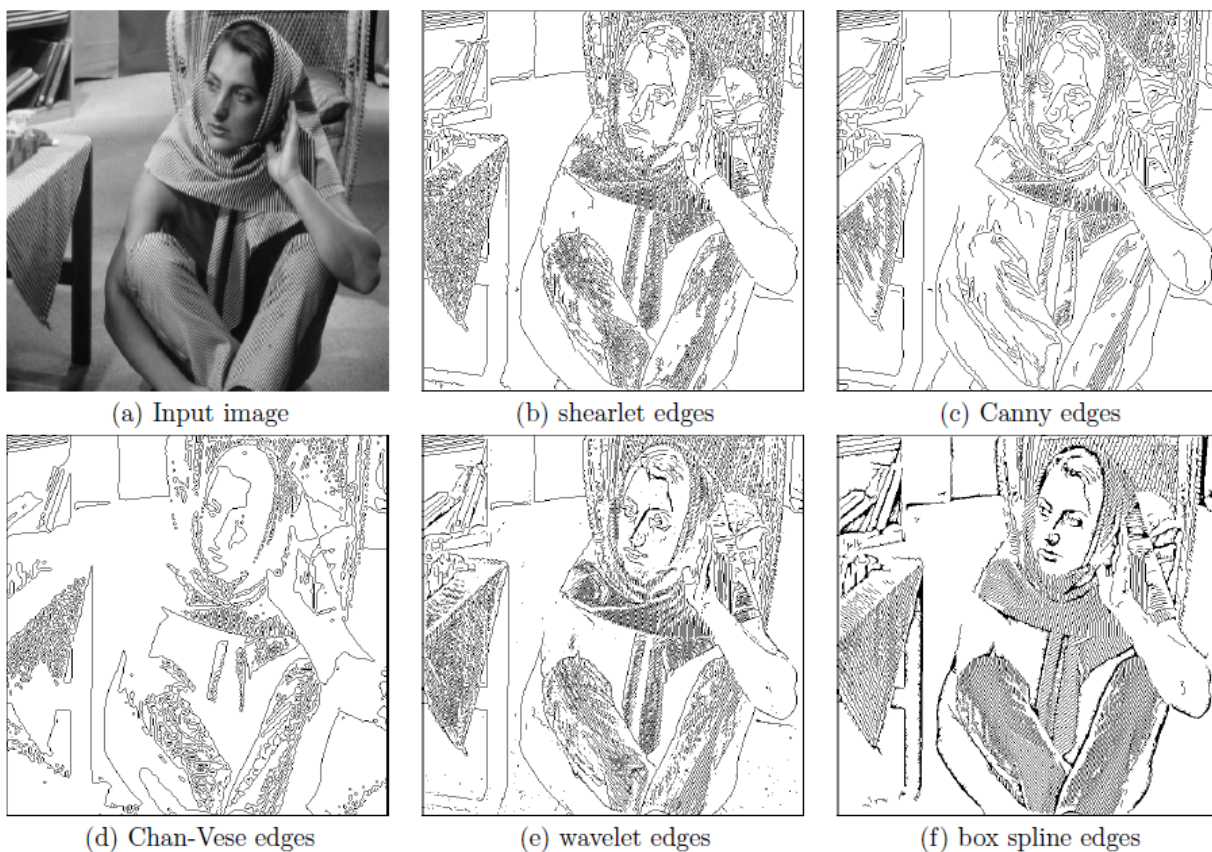


Figure 1: An example of image simplification by using box spline based tight-wavelet frames courtesy of Ming-Jun Lai, an author of [13].

2 Image Simplification

It is crucial to simplify the images, so that we can keep the important features in an image while removing the noises before we feed them into any machine learning model for image classification. It is well-known that we can use the standard PCA to simplify an image. In fact, we have tried to use the first 10 singular values of each image to build up an adjacency matrix A , however, it turns out that the numerical results of image classification based on PCA simplification does not work very well. We thus turned to other approaches.

We now explain the box spline-based tight-wavelet frames, called LN method, to simplify these images. The tight wavelet frames (TWF) we used in this paper were constructed in [24] based on integer translations of box spline B_{2211} (cf. [5] and [19]). Dr. Kyunglim Nam implemented the constructive method in [21] based on box spline B_{2211} to construct tight-wavelet framelets for image decomposition and reconstruction. In fact, she constructed tight-wavelet frames based on other box splines. See her dissertation [24] for more detail. Her MATLAB codes were further revised by Dr. Ming-Jun Lai with a denoising technique to have a package called LNmethod.m. As shown in Figure 1, we can easily see the box spline-based tight-wavelet frames method outperforms other traditional edge detection approaches and is able to capture and enhance the edge features across all directions in the image. More recent study can be found in [13].

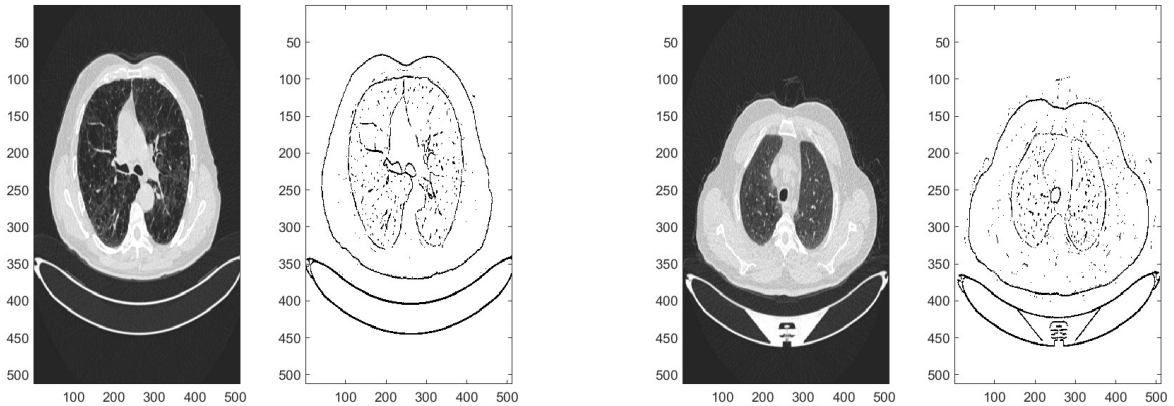


Figure 2: Two examples of lung image simplification based on LN method.

The main idea of LN method is to decompose an image into its low frequency part and high frequency part by using the tight-wavelet frames and then reconstruct the high frequency part back based only on the high-pass frequency part without the low-pass frequency. The resulting image is noisy and is denoised by using a cutoff parameter which is dependent on each image. We find an intelligent way to let the computer decide the best parameter to clean each of the medical images of interest. Let us present some examples of medical image simplification by using the LN method in Figure 2.

3 Generation of Adjacency Matrices

Let us now explain the way we build the adjacency matrices for our graph clustering approach. We mainly use the distance associated with Gaussian kernel with different parameters to generate a working adjacency matrix. Let us call it *Modified Exponential Distance*:

Let $\mathbf{x}_i \in \mathbb{R}^n$ be the vectorization of each image from the original data set and $NN(\mathbf{x}_i, K)$ is the set of K -nearest neighbors of \mathbf{x}_i . For $r \geq 1$, let $\sigma_i = \|\mathbf{x}_i - \mathbf{x}^{i,r}\|$ be the r -th closest point of \mathbf{x}_i . We build the adjacency matrix associated with the data set to be $A = [A_{ij}]_{i,j=1,\dots,n}$ with entries

$$A_{ij} = \begin{cases} \exp(-\|\mathbf{x}_i - \mathbf{x}_j\|/(\sigma_i\sigma_j)) & \text{if } \mathbf{x}_j \in NN(\mathbf{x}_i, K) \\ 0 & \text{otherwise} \end{cases} \quad (3)$$

for all $i, j = 1, \dots, n$ (cf. [34]).

Note that the above A_{ij} is not necessarily symmetric, so we consider $\tilde{A}_{ij} = A^\top A$ for symmetrization. Alternatively, one may also use $\tilde{A}_{ij} = \max\{A_{ij}, A_{ji}\}$ or $\tilde{A}_{ij} = (A_{ij} + A_{ji})/2$.

Based on the modified exponential distance (3), we generate the adjacency matrix with the choice of two parameters r and K over all the images. The ideal adjacency matrix would have a block diagonal structure where each block corresponds to one class in the dataset.

Once we have the way to generate the adjacency matrix, we can use the LN method explained before to simplify the given medical images and use the modified exponential distance with the same parameters to build a much cleaner adjacency matrix. The two adjacency matrices, without and with the LN method, are shown in Figure 3. It is easy to see that the adjacency matrix based on LN method is much cleaner than the adjacency matrix built from the original images.

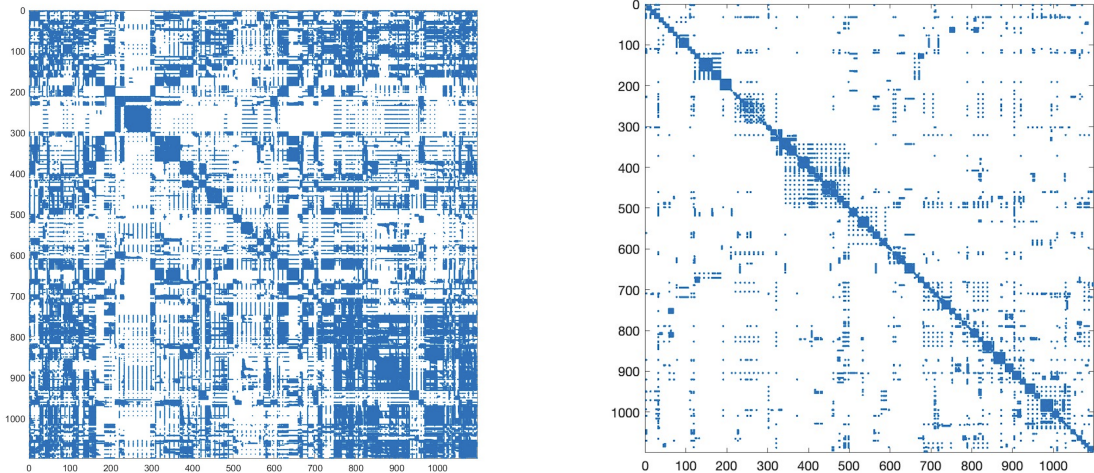


Figure 3: Adjacency matrices built without (left) and with the LN method (right) based on a Modified Exponential Distance.

4 Local Clustering Based on Sparse Solution Technique

Let us present the idea of two local clustering methods [20] and [28]. Recall that if a graph G has k connected components C_1, \dots, C_k , then its graph Laplacian \mathcal{L} can be written into block diagonal form

$$\mathcal{L} = \begin{bmatrix} \mathcal{L}_1 & & & \\ & \mathcal{L}_2 & & \\ & & \ddots & \\ & & & \mathcal{L}_k \end{bmatrix}, \quad (4)$$

with each \mathcal{L}_i being the graph Laplacian of the i -th component. It is known that the indicators $\mathbf{c}_1, \dots, \mathbf{c}_k$, which are associated with the clusters C_1, \dots, C_k , are in the null space of the kernel of \mathcal{L} . That is, $\mathcal{L}\mathbf{c}_i = 0, i = 1, \dots, k$ (cf. [6] and [23]).

Note that $\|\mathbf{c}_i\|_0 \ll n$, where $\|\mathbf{x}\|_0$ is the number of nonzero components in \mathbf{x} . Then we can find such component by solving the following minimization problem:

$$\min \|\mathbf{x}\|_0, \quad \mathcal{L}\mathbf{x} = 0, \quad \mathbf{x} \neq \mathbf{0}. \quad (5)$$

In practice, the graphs are usually "noised", and thus we may not be able to find an exact solution \mathbf{x} . However, as long as the noise is small enough, the output solution based on the perturbed version of \mathcal{L} should be close to the exact solution.

To avoid getting zero vector as a solution, we also remove a collection T of columns from all columns V and solve for

$$\arg \min_{\mathbf{x} \in \mathbb{R}^{|V|-|T|}} \{\|\mathcal{L}_{V \setminus T}\mathbf{x} - \mathbf{y}\|_2 : \|\mathbf{x}\|_0 \leq s\}, \quad (6)$$

where s is the sparsity constraint assumption for \mathbf{x} , and \mathbf{y} is the row sum vector of $\mathcal{L}_{V \setminus T}$. We present the detailed procedure for this method, named Local Cluster Extraction (LCE), as Algorithm 1.

Another similar computational algorithm proposed in [20] is to simply drop the sparsity constraint in (6), hence we will solve a least squares problem. We name the method Least Squares Clustering (LSC) and present it as Algorithm 2. There are many algorithms available that solve the minimizations (5) and (6). We refer the interested reader to several other methods in [22].

Algorithm 1 Local Cluster Extraction [28]

Input: Adjacency matrix A , and a small set of seeds $\Gamma \subset C_1$

Parameter: Estimated size $\hat{n}_1 \approx |C_1|$, random walk threshold parameter $\epsilon \in (0, 1)$, random walk depth $t \in \mathbb{Z}^+$, sparsity parameter $\gamma \in [0.1, 0.5]$, rejection parameter $R \in [0.1, 0.9]$.

Output: The target cluster C_1

- 1: Compute $P = AD^{-1}$, $\mathbf{v}^0 = D\mathbf{1}_\Gamma$, and $L = I - D^{-1}A$.
- 2: Compute $\mathbf{v}^{(t)} = P^t\mathbf{v}^{(0)}$.
- 3: Define $\Omega = \mathcal{L}_{(1+\epsilon)\hat{n}_1}(\mathbf{v}^{(t)})$.
- 4: Let T be the set of column indices of $\gamma \cdot |\Omega|$ smallest components of the vector $|L_\Omega^\top| \cdot |L\mathbf{1}_\Omega|$.
- 5: Set $\mathbf{y} := L\mathbf{1}_{V \setminus T}$. Let $\mathbf{x}^\#$ be the solution to

$$\arg \min_{\mathbf{x} \in \mathbb{R}^{|V|-|T|}} \{ \|L_{V \setminus T}\mathbf{x} - \mathbf{y}\|_2 : \|\mathbf{x}\|_0 \leq (1 - \gamma)\hat{n}_1 \} \quad (7)$$

obtained by using $O(\log n)$ iterations of *Subspace Pursuit* [8].

- 6: Let $W^\# = \{i : \mathbf{x}_i^\# > R\}$.
 - 7: **return** $C_1^\# = W^\# \cup T$.
-

Let us first present two examples of clustering human faces to demonstrate that our local clustering based on sparse solution methods works very well.

Example 1 *The AT&T human faces dataset [26] contains grayscale images for 40 different people of pixel size 56×46 . Images of each person are taken under 10 different conditions, by varying the three perspectives of faces, lighting conditions, and facial expressions. As shown in Figure 4, we use part of this dataset and use the modified exponential distance function explained before and then apply LCE and LSC to extract the faces into their correct clusters.*

Example 2 *The "Extended Yale Face Database B (YaleB)" [11] dataset contains 16128 grayscale images of 28 human subjects under 9 poses and 64 illuminations. We use the modified exponential distance function explained before and then apply LCE and LSC to extract the faces into their correct clusters. See Figure 5 for the illustration.*

5 Experiments

5.1 Dataset Description

We carried out the experiments on the "Iraq-Oncology Teaching Hospital/National Center for Cancer Diseases (IQ-OTH/NCCD)" lung cancer dataset. The dataset was collected from the "Iraq-Oncology Teaching Hospital and the National Center for Cancer Diseases" for more than three months in 2019. It consists of CT scans from patients, including both healthy individuals and those diagnosed with various stages of lung cancer. The dataset, annotated by multiple oncologists and radiologists, consists of 1,097 CT scan images of the human chest. These images represent 110 cases (40 identified as malignant, 15 as benign, and 55 as normal), with variations in age, gender, educational background, residence, and living conditions. The cases in this study were divided into three categories: benign, malignant, and normal, as depicted in Figure 6. The IQ-OTH/NCCD dataset can be downloaded from the website such as [4] on Kaggle. The breakdown of the distribution of this dataset by class-wise category is presented in Table 1.

Algorithm 2 Least Squares Clustering [20]

Input: Adjacency matrix A , and a small set of seeds $\Gamma \subset C_1$.

Parameter: Estimated size $\hat{n}_1 \approx |C_1|$, random walk threshold parameter $\epsilon \in (0, 1)$, random walk depth $t \in \mathbb{Z}^+$, least squares threshold parameter $\gamma \in (0, 1)$, rejection parameter $R \in [0.1, 0.9]$.

Output: The target cluster C_1

- 1: Compute $P = AD^{-1}$, $\mathbf{v}^0 = D\mathbf{1}_\Gamma$, and $L = I - D^{-1}A$.
- 2: Compute $\mathbf{v}^{(t)} = P^t\mathbf{v}^{(0)}$.
- 3: Define $\Omega = \mathcal{L}_{(1+\epsilon)\hat{n}_1}(\mathbf{v}^{(t)})$.
- 4: Let T be the set of column indices of $\gamma \cdot |\Omega|$ smallest components of the vector $|L_\Omega^\top| \cdot |L\mathbf{1}_\Omega|$.
- 5: Set $\mathbf{y} := L\mathbf{1}_{\Omega \setminus T}$. Let $\mathbf{x}^\#$ be the solution to

$$\arg \min_{\mathbf{x} \in \mathbb{R}^{|\Omega| - |T|}} \|L_{\Omega \setminus T}\mathbf{x} - \mathbf{y}\|_2 \quad (8)$$

obtained by using an iterative least squares solver.

- 6: Let $W^\# = \{i : \mathbf{x}_i^\# > R\}$.
 - 7: **return** $C_1^\# = \Omega \setminus W^\#$.
-

Table 1: The class-wise distribution of the “IQ-OTH/NCCD” lung cancer dataset.

Class	Patients	No. of Samples
Benign	15	120
Malignant	40	561
Normal	55	416
Total	110	1097

5.2 Experimental Procedure

Let us now explain the experimental procedure to identify whether a given lung cancer image is benign, malignant, or normal.

First of all, we preprocess the data by scaling all the images into the standard size of 512×512 as the given image data are not in a uniform size. Then we experimented with various image simplification methods, e.g. PCA, LN method, Watershed, etc.. It turns out that the LN method can work nicely. One of the mathematical heuristics is that each image has a lot of redundant information, e.g. the pixel values outside of the cross-section of the lung of a person which may inference the similarity of the two images.

After preprocessing and simplifying the image data, we can build the adjacency matrix using modified exponential distance. Let us outline our algorithm for identification of each individual image. Our image identification procedure is summarized as Algorithm 3.

We apply LCE or LSC on the adjacency matrix which is built by using the modified exponential distance between each testing image and the remaining images with known labels. In the experiments, we randomly select 10 benign images, 50 malignant images, 40 normal images (roughly follow the distribution of the dataset), a total of 100 images out of 1097 images as testing images. For each individual testing image, we perform Algorithm 3 to determine its class label. Note that the last step in Algorithm 3 is based on the majority vote. For example, if the cluster (after excluding the testing image itself) is of size 10, which contains 2 images with label benign, 5 images with label malignant, 3 images with label normal, then this testing image is classified as malignant. The experiments are



Figure 4: Given a set of faces (left), we sorted these faces (right) which were done by using LCE or LSC.

Algorithm 3 Image Identification

- 1: Given an individual testing (query) image S , we build the adjacency matrix by using modified exponential distance between the testing image and the remaining images with known labels.
 - 2: Apply the LCE or LSC algorithm with the seed S to output a cluster C_S of small size, e.g., size of 10.
 - 3: Conclude that S belong to a certain class (benign, malignant, normal) if that class label appears the most (after excluding S itself) in C_S .
-

conducted over 100 repetitions. The code which can reproduce our experimental results is available on <https://github.com/zzzms/LocalClustering4LungCancer>.

5.3 Evaluation Metrics and Benchmarks

We propose to use evaluation metrics, including Accuracy, Precision, Recall, F1-score, and confusion matrix to validate the performance of our approach. Comparisons are conducted on benchmark methods including the KNN (k-Nearest neighbors) [1], integrated contrast/features-based method (CFM) [15], weakly supervised deep learning (WSDL) [30], Co-learning feature fusion maps (CLFM) [16], DFD-Net [29], and CNN-SOA [32].

5.4 Hyperparameters

For both the IQ-OTH/NCCD and Pneumonia dataset, we set $K = 5$ and $r = 3$ to generate the adjacency matrix based on modified exponential distance.

For LCE method on IQ-OTH/NCCD dataset, we set random walk threshold parameter to be 0.8,

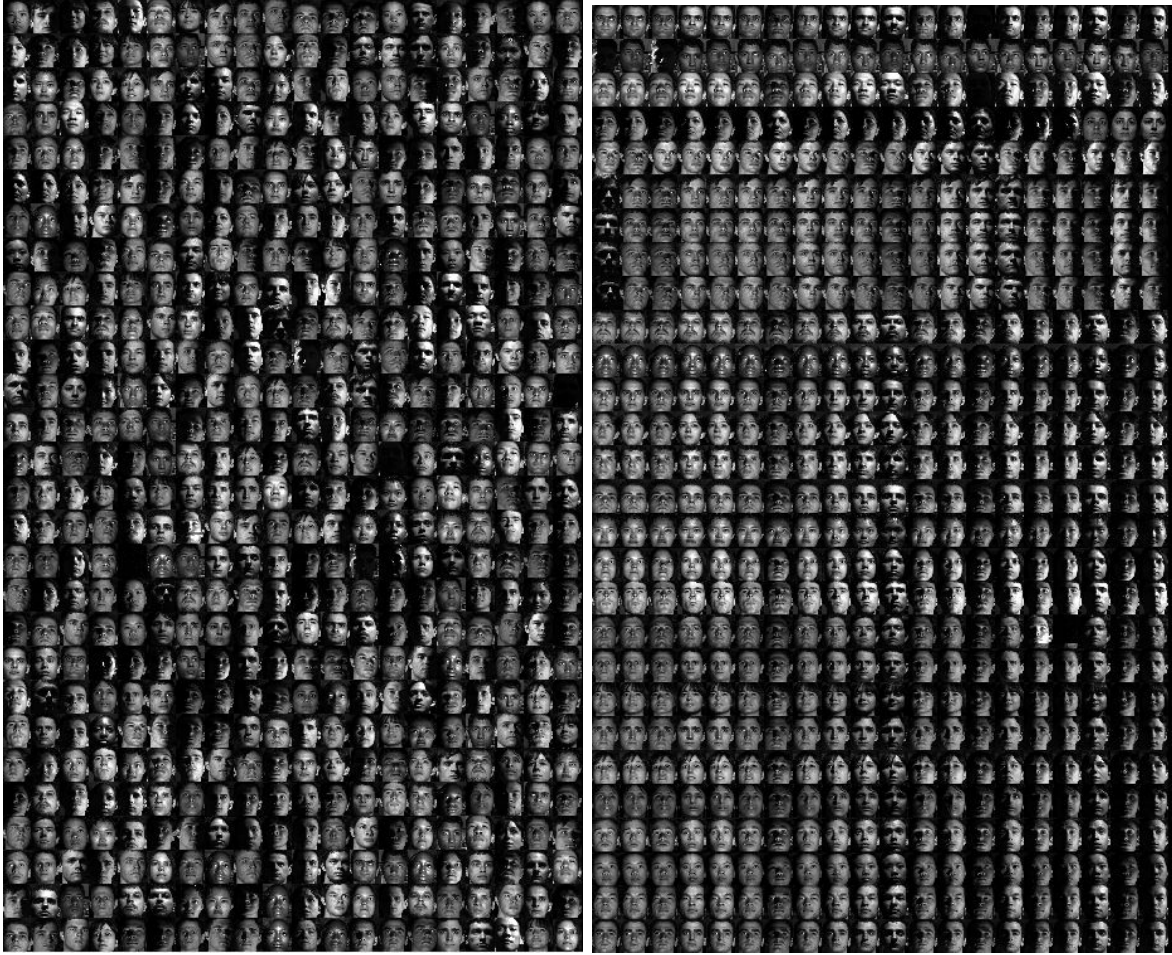


Figure 5: Given a set of faces (left), we sorted these faces (right) which were done by using LCE or LSC.

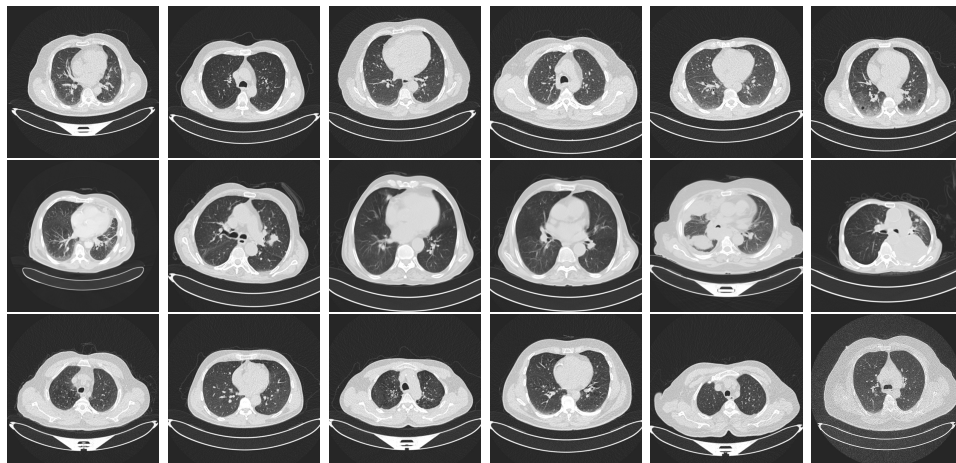


Figure 6: Examples of benign cases (top row), malignant cases (middle row), and normal cases (bottom row).

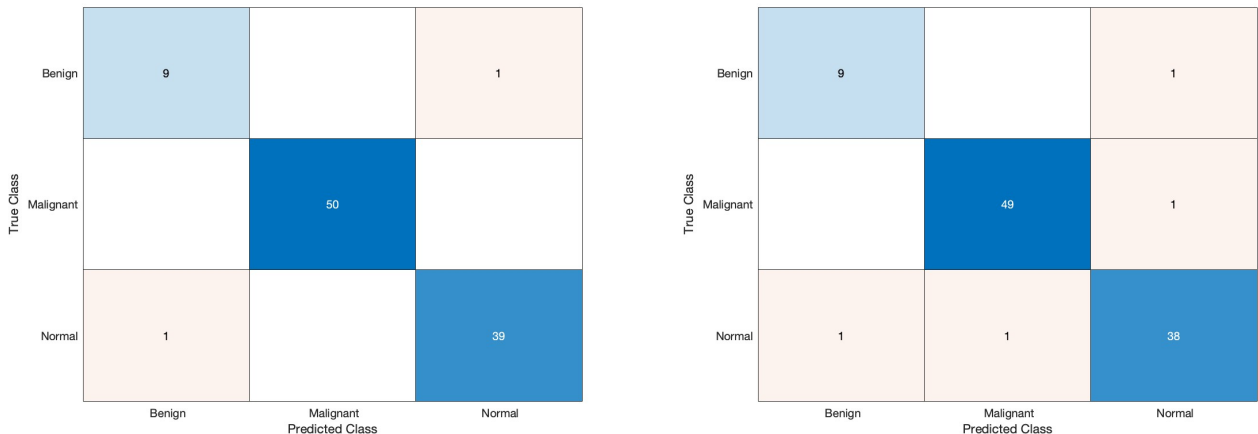


Figure 7: Confusion matrix of LCE (left) and LSC (right) on IQ-OTH/NCCD dataset. The values are rounded to integers.

Table 2: Precision/Recall/F1-score of Image Identification by Two Local Clustering Methods

	LCE	LSC
Benign	87.98 / 87.80 / 87.89	85.38 / 88.80 / 87.06
Malignant	98.90 / 99.34 / 99.12	97.59 / 98.10 / 97.84
Normal	96.86 / 96.37 / 96.61	95.65 / 94.08 / 94.86

random walk depth to be 3, sparsity parameter to be 0.2, rejection parameter to be 0.0. The estimated size of output cluster is set to be 6. For LCE method on Pneumonia dataset, everything else is the same except that the output cluster is set to be 8.

For LSC method on both IQ-OTH/NCCD and Pneumonia dataset, we set random walk threshold parameter to be 0.2, random walk depth to be 3, sparsity parameter to be 0.2, least squares threshold parameter to be 0.2, rejection parameter to be 0.9. The estimated size of output cluster is set to be 10.

5.5 Results

We show the average confusion matrix over 100 runs of LCE and LSC methods in Figure 7, note that the entries in the confusion matrix are rounded to be integers. The overall accuracy (\pm standard deviation) for LCE and LSC on Pneumonia dataset are $97.10\% \pm 1.71\%$ and $95.56\% \pm 2.10\%$ respectively. The performances of the two proposed methods are presented in Table 2, and the comparisons with the other benchmarks are summarized in Table 3. Note that the precision, recall, and F1-score in Table 3 are the macro-average values over the entire dataset.

Furthermore, we compare our methods with several other modern deep learning approaches such as EfficientNetB0, GoogleLeNet, ResNet50, EfficientNetB4, Attention-InceptionResNet-V2, and MobileNetV2. According to [25], the testing accuracy for these deep neural network based approaches are 93.67%, 94.38%, 94.40%, 97.29%, 97.41%, 98.28% respectively. The accuracy of LCE and LSC in Table 3 are comparable to these state-of-the-art results. It is worthwhile to point out that LCE and LSC require no training and the identification of 100 testing images only takes about a few seconds, while the neural network approaches usually take about hours for training plus testing.

Table 3: Performance of the two local clustering methods compared with other benchmarks (the best results are in bold and second best results are underlined)

	Accuracy	Precision	Recall	F1-score
LCE (ours)	97.10	94.58	<u>94.50</u>	94.54
LSC (ours)	95.56	<u>92.87</u>	93.66	<u>93.25</u>
KNN [1]	85.25	71.09	85.32	82.56
CFM [15]	87.24	75.94	87.24	84.19
WSDL [30]	89.26	78.26	89.16	86.37
CLFM [16]	92.46	81.39	91.08	88.34
DFD-Net [29]	94.52	83.50	93.65	89.90
CNN-SOA [32]	<u>96.58</u>	84.16	95.38	91.35

6 Final Remarks

Let us conclude the paper with few remarks. An additional dataset has been used for experiment and we report some results in the first subsection. Then we remark on how to obtain more labeled image data to further improve our proposed methods.

6.1 More Experimental Results

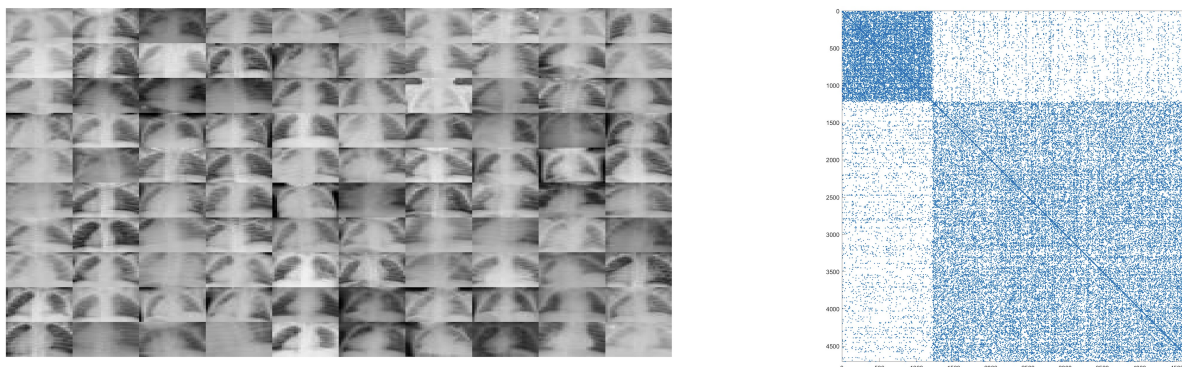


Figure 8: A Few Sample Images (left) and an Adjacency Matrix A (right) associated with the Pneumonia Image Data

In addition to the “IQ-OTH/NCCD” lung cancer dataset, we used the Pneumonia patient images from [33], which is a collection of MNIST-like images for more experiments. The dataset consists 4708 images (we only use the training part of this dataset), where 1214 are normal and 3494 are malignant. Therefore it is a binary classification problem. A small samples of images are shown in Figure 8. We again use the modified exponential distance function to generate an adjacency matrix, which has very nice block structure as shown in Figure 8. Therefore no LN method is needed for this dataset.

We randomly choose 100 images (25 normal, 75 malignant) out of the 4708 images as testing samples. For each testing image, we apply LCE or LSC on the adjacency matrix which is built by using modified exponential distance between the testing image and the remaining images with known labels. The size of output cluster are set to be 8 for LCE (or 10 for LSC), after excluding the seeded testing image, the cluster is of size 7 for LCE (or 9 for LSC).

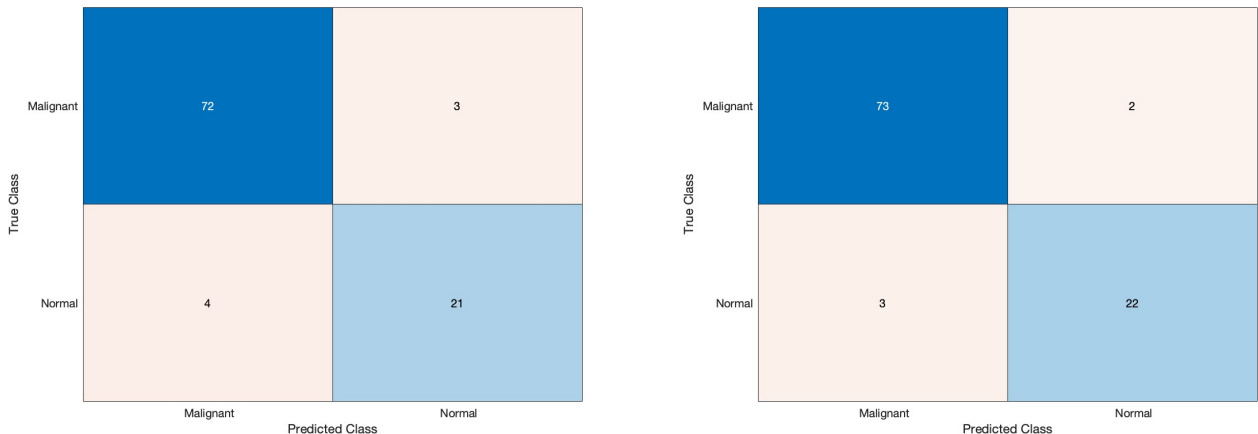


Figure 9: Confusion matrix of LCE (left) and LSC (right) on Pneumonia dataset. The values are rounded to integers.

Table 4: Precision/Recall/F1-score of Image Identification by the two methods on Pneumonia Dataset

	Malignant	Normal
LCE	95.99 / 94.68 / 95.33	84.67 / 88.12 / 86.38
LSC	96.05 / 97.33 / 96.69	89.68 / 86.16 / 87.88

The labels of these images in the output cluster are used to determine the label of the testing image. If more than half of the labels are normal, we conclude the corresponding testing image as normal. Otherwise, we conclude the corresponding testing image as malignant.

Figure 9 gives the confusion matrix over 100 independent repetitions of the experiment. Note that the entries in the confusion matrix are rounded to be integers. In Table 4, we show the average precision, recall, and F1-score for each category over 100 independent repetitions of the experiment. The overall accuracy (\pm standard deviation) for LCE and LSC on Pneumonia dataset are $93.04\% \pm 2.45\%$ and $94.06\% \pm 2.17\%$ respectively, while the performances of other benchmark approaches on this dataset are auto-sklearn 85.5%, AutoKeras 87.8%, ResNet50 88.4%, GoogleAutoMLVision 94.6% (cf. [33]). Therefore, our proposed local clustering methods can achieve a favorable or comparable results with much less computational cost.

6.2 More Artificially Generated Labeled Images

One direction to improve the performance of the proposed LCE and LSC methods is to generate more artificial images, i.e., increase the number of labeled data, hence the proposed methods will be more likely to find a faithful cluster. We propose two approaches to do so.

One approach for generating more labeled data is based on the numerical solution to the Monge-Ampère equation (cf. [17]) for the optimal transport problem. That is, we deform the portion over the chest of each image in the malignant class to the portion of the chest in each image in the normal class. There are a few computational difficulties to overcome such as identifying the centers of the domains of the chests. We shall leave the details to a future publication. Another approach is to use the method of harmonic generalized barycentric coordinates (GBC) to do the image deformation. See [9] and [14] for some examples of image deformation. Let us illustrate this idea by Figures 10, 11,

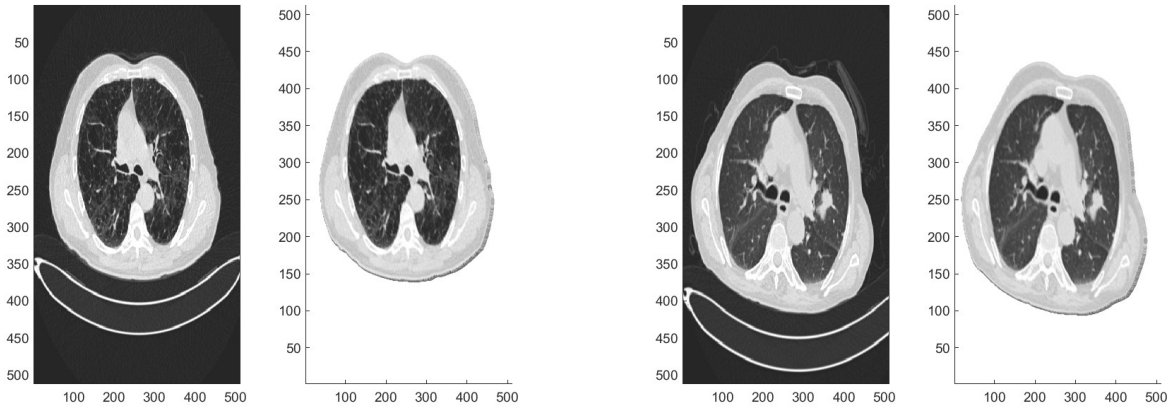


Figure 10: The chest of a test image (leftmost), the domain V of interest (second from left), the chest of a malignant image (third from left) and the domain W of interest (rightmost)

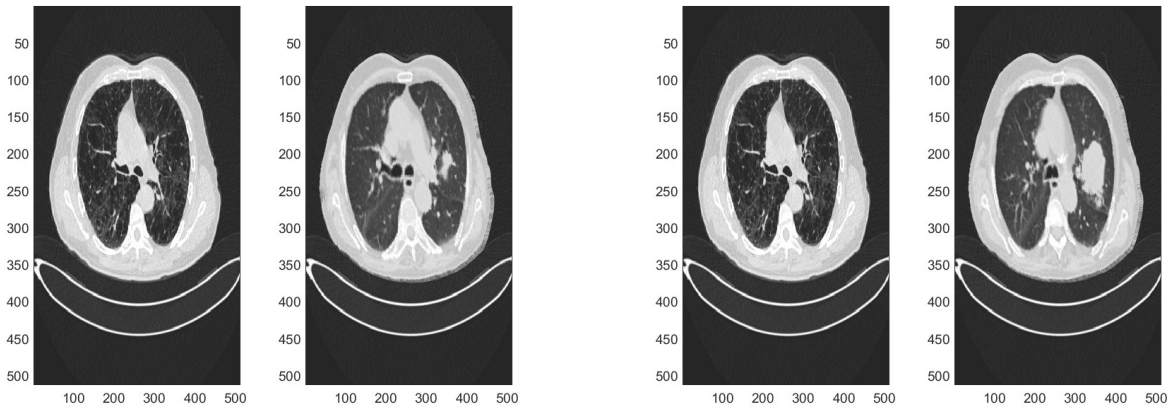


Figure 11: The chest of the test image (leftmost), the chest with malignant lung (second from left) after the GBC deformation, and another pair of the test image and the deformed image using another malignant lung (right).

and 12.

The idea is, we first isolate the chest of each medical image as shown in Figure 10 from the most left one to the second left one and similarly from the third left to the most right one. Let V be the domain of interest in the second from left in Figure 10, and W be the domain on the right of Figure 10. We deform W to V by using the so-called harmonic GBC method as discussed in (cf. [9] and [14]). This results in the image on the second from the left of Figure 11. We can see that the resulting image is a new chest image with a malignant lung. Similarly, we can use the method to obtain many more examples of malignant lung cases in different chest images via deformation, as shown in Figure 11 and Figure 12. We can do such deformation between all pairs of malignant, benign, and normal images. In this way, we will obtain more than ten thousand labeled images.

If a test image has a similar chest to one of the images in the normal class but has a malignant lung resembling that in one of malignant cases, our local clustering methods will be able to identify it as a malignant case. Even if a testing image has a chest different in silhouette from all existing labeled images, we can deform all the chests from the images in the malignant class to the chest of the testing

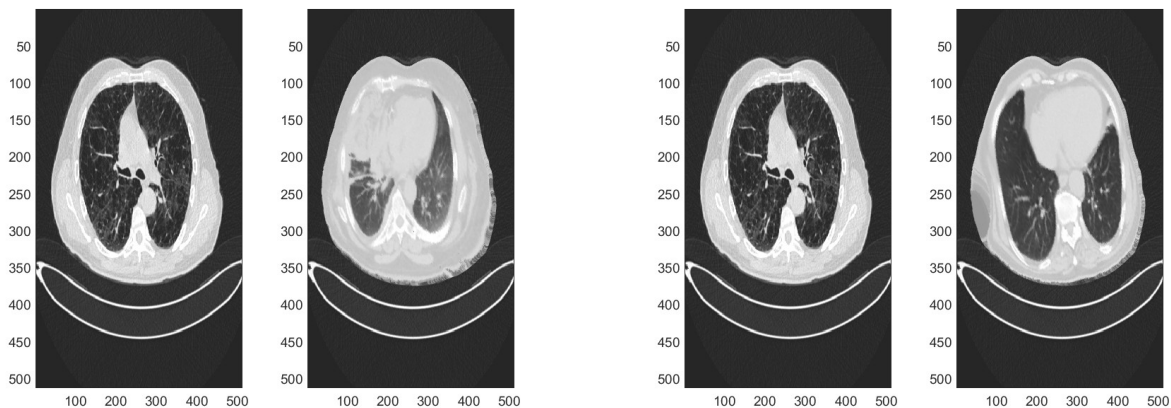


Figure 12: More examples of the chest images with malignant lungs deformed to the chest of the test image.

image. Then we use our approach to find if the testing image should be labeled a malignant image or not.

The goal of our idea above is to deform, via the GBC deformation or Optimal transportation, more than 500 chest images with malignant lungs to the chest image in the test. Our method will determine whether the lung area in the testing image resembles any of the malignant cases, much like the process of doctors making diagnoses based on their experiences, i.e. the memory of thousands of images of malignant lungs, the deformation of these malignant lungs into the test chest, and the comparison of the testing image to make a diagnosis. On the other hand, we will have more than 10,000 labeled images by deforming all malignant lungs and benign lungs to each of normal lungs as artificially labeled images for training. We leave the generation of these images over the entire dataset to future work.

Acknowledgment

The second author is supported by the Simons Foundation for collaboration grant #864439. The authors would like to thank the reviewers for their constructive comments and suggestions.

References

- [1] M. F. Abdullah et al., Classification of Lung Cancer Stages From CT Scan Images Using Image Processing and K-Nearest Neighbours, pages 68–72 IEEE, 2020.
- [2] F. Ahmed et al., Topo-CXR: Chest X-ray TB and pneumonia screening with topological machine learning, In 2023 IEEE/CVF International Conference on Computer Vision Workshops (ICCVW), pages 2318–2328. IEEE, 2023.
- [3] M. S. Al-Huseiny and A. S. Sajit. “Transfer learning with GoogLeNet for detection of lung cancer.” Indonesian Journal of Electrical Engineering and computer science 22.2 (2021): 1078-1086.
- [4] H. F. Al-Yasriy, IQ-OTH/NCCD - Lung Cancer Dataset. 2020; Available from: <https://www.kaggle.com/datasets/adityamahimkar/iqothnccd-lung-cancer-dataset>.

- [5] C. de Boor, K. Höllig, and S. Riemenschneider, Box Splines, Springer Verlag, 1993.
- [6] F. Chung, Spectral Graph Theory, American Mathematical Society, 1997.
- [7] E. J. Candes, J. Romberg, and T. Tao. Robust uncertainty principles: Exact signal reconstruction from highly incomplete frequency information. *IEEE Transactions on Information Theory*, 52(2):489–509, 2006
- [8] W. Dai and O. Milenkovic. Subspace pursuit for compressive sensing signal reconstruction. *IEEE Transactions on Information Theory*, 55(5):2230–2249, 2009.
- [9] C. Deng, T.-W. Hu, and M.-J. Lai, The Harmonic GBC Function Map is a Bijection if the Target Domain is Convex, submitted, (2022).
- [10] D. L. Donoho, Compressed sensing. *IEEE Transactions on Information Theory*, 52(4):1289–1306, 2006.
- [11] A. S. Georghiadis, P. N. Belhumeur, and D. J. Kriegman, From few to many: Illumination cone models for face recognition under variable lighting and pose. *PAMI*, 23:643–660, 2001.
- [12] B. Halalli and A. Makandar. Computer-aided diagnosis-medical image analysis techniques, *Breast imaging*, 85:85–109, 2018.
- [13] W. Guo and M.-J. Lai, Box Spline Wavelet Frames for Image Edge Analysis, *SIAM Journal Imaging Sciences*, vol. 6 (2013) pp. 1553–1578.
- [14] T.-W. Hu, Computational Methods for Smooth Mapping and Interpolation using Multivariate Spline Techniques, Dissertation, University of Georgia, May 2023.
- [15] M. A. Khan et al., Lungs cancer classification from CT images: An integrated design of contrast based classical features fusion and selection, *Pattern Recogn. Lett.* 129 (2020) 77–85.
- [16] A. Kumar et al., Co-learning feature fusion maps from PET-CT images of lung cancer, *IEEE Trans. Med. Imaging* 39 (1) (2019) 204–217.
- [17] M.-J. Lai and J. Lee, A Bivariate Splines based Collocation Method for Numerical Solution to Optimal Transport Problem, submitted, (2024).
- [18] M.-J. Lai and D. McKenzie, Compressive sensing for cut improvement and local clustering. *SIAM Journal on Mathematical Data Science*, 2, (2020) pp. 368–395.
- [19] M.-J. Lai and L. L. Schumaker, Spline Functions on Triangulations, Cambridge University Press, 2007.
- [20] M.-J. Lai and Z. Shen. “A compressed sensing based least squares approach to semi-supervised local cluster extraction.” *Journal of Scientific Computing* 94, no. 3 (2023): 63.
- [21] M.-J. Lai and J. Stöckler, Construction of Multivariate Compactly Supported Tight Wavelet Frames, *Applied and Computational Harmonic Analysis*, vol. 21 (2006) pp. 324–348.
- [22] M.-J. Lai and Y. Wang, Sparse Solutions of Underdetermined Linear Systems and Their Applications, *SIAM Publication*, 2021.
- [23] U. von Luxburg, A Tutorial on Spectral Clustering, *Stat. Comput.* 17(2007), 395–416.

- [24] K. Nam, Tight Wavelet Frame Construction and Its Application for Image Processing, Dissertation, University of Georgia, 2005.
- [25] R. Raza et al. "Lung-EffNet: Lung cancer classification using EfficientNet from CT-scan images." *Engineering Applications of Artificial Intelligence* 126 (2023): 106902.
- [26] F. S. Samaria and A. C. Harter, Parameterisation of a stochastic model for human face identification, *Proceedings of 2nd IEEE Workshop on Applications of Computer Vision*, 1994.
- [27] Z. Shen, "Sparse Solution Technique in Semi-supervised Local Clustering and High Dimensional Function Approximation." Ph.D. dissertation, University of Georgia, May 2024
- [28] Z. Shen, M.-J. Lai, and S. Li. "Graph-based semi-supervised local clustering with few labeled nodes." In *Proceedings of the Thirty-Second International Joint Conference on Artificial Intelligence*, pp. 4190-4198. 2023.
- [29] W. J. Sori et al., DFD-Net: lung cancer detection from denoised CT scan image using deep learning, *Front. Comp. Sci.* 15 (2) (2021) 1–13.
- [30] X. Wang et al., Weakly supervised deep learning for whole slide lung cancer image analysis, *IEEE Trans. Cybern.* 50 (9) (2019) 3950–3962.
- [31] A. Yadav, F. I. Ahmed, O. Daescu, R. Gedik, and B. Coskunuzer, Histopathological cancer detection with topological signatures. In *2023 IEEE International Conference on Bioinformatics and Biomedicine (BIBM)*, pages 1610–1619, IEEE, 2023.
- [32] C. Yan and N. Razmjoooy, "Optimal lung cancer detection based on CNN optimized and improved Snake optimization algorithm." *Biomedical Signal Processing and Control* 86 (2023): 105319.
- [33] J. Yang et al. MedMNIST v2 - A large-scale lightweight benchmark for 2D and 3D biomedical image classification. *Sci Data* 10, 41 (2023).
- [34] L. Zelnik-Manor and P. Perona, Self-tuning spectral clustering. In *Advances in Neural Information Processing Systems*, pages 1601–1608, 2004.
- [35] S. K. Zhou et al., A review of deep learning in medical imaging, *Proceedings of the IEEE*, 109(5): 820–838, 2021.